energy&fuels

pubs.acs.org/EF

Article

Ceramic–Polymer–Carbon Composite Coating on the Truncated Octahedron-Shaped LNMO Cathode for High Capacity and Extended Cycling in High-Voltage Lithium-Ion Batteries

Sivaraj Pazhaniswamy,* Gihoon Cha, Sagar A. Joshi, Abhilash Karuthedath Parameswaran, Rajan Jose, Sabrina Pechmann, Silke Christiansen, and Seema Agarwal*

Cite This: *Energy Fuels* 2024, 38, 21456–21467

Read Online

ACCESS | Metrics & More | Article Recommendations | Supporting Information

ABSTRACT: Long-term electrochemical cycle life of the $LiNi_{0.5}Mn_{1.5}O_4$ (LNMO) cathode with liquid electrolytes (LEs) and the inadequate knowledge of the cell failure mechanism are the eloquent Achilles' heel to practical applications despite their large promise to lower the cost of lithium-ion batteries (LIBs). Herein, a strategy for engineering the cathode–LE interface is presented to enhance the cycle life of LIBs. The direct contact between cathode-active particles and LE is controlled by encasing sol–gel-synthesized truncated octahedron-shaped LNMO particles by an ion–electron-conductive (ambipolar) hybrid ceramic–polymer electrolyte (IECHP) via a simple slot-die coating. The IECHP-coated LNMO cathode demonstrated negligible capacity fading in 250 cycles and a capacity retention of ∼90% after 1000 charge–discharge cycles, significantly exceeding that of the uncoated LNMO cathode (a capacity retention of ∼57% after 980 cycles) in 1 M $LiPF_6$ in EC:DMC at 1 C rate. The difference in stability between the two types of cathodes after cycling is examined by focused ion beam scanning electron microscopy and time-of-flight secondary ion mass spectrometry. These studies revealed that the pristine LNMO produces an inactive layer on the cathode surface, reducing ionic transport between the cathode and the electrolyte and increasing the interface resistance. The IECHP coating successfully overcomes these limitations. Therefore, the present work underlines the adaptability of IECHP-coated LNMO as a high-voltage cathode material in a 1 M $LiPF_6$ electrolyte for prolonged use. The proposed strategy is simple and affordable for commercial applications.

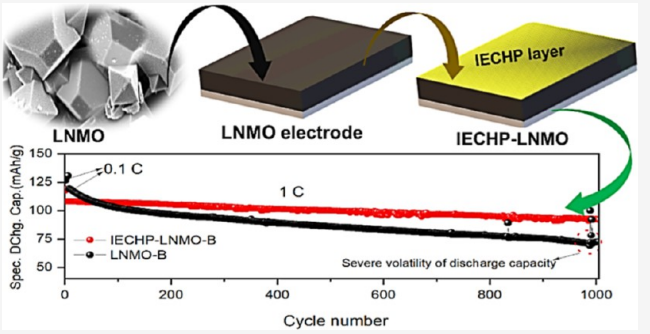

1. INTRODUCTION

Long-term cycle stability and high energy density are significant characteristics of lithium-ion batteries (LIBs), which are highly explored in electric vehicles (EVs) and grid energy storage.[1,2] However, the present LIB technology is no longer able to meet market demand. The specific capacity and operating voltage of the cathode-active materials have a substantial influence on LIB's energy density and cycle performance. By definition, energy = capacity × voltage, which opens two ways to enhance the energy density of LIBs: by raising the specific capacity of cathode materials and by increasing the upper limit of charging voltage.[3] The development of new cathode materials of high specific capacity (>275 mA h g^{-1}) with an increased nickel content in the layered transition metal oxide cathode materials or designing innovative active material compositions is particularly challenging.[3,4] Hence, increasing the upper voltage limit of the cathode material is much easier to enhance the energy density of LIBs. Despite the advantages of high cutoff voltage, an exorbitant upper-limit charging voltage severely degrades various battery components, including side reactions, transition metal dissolution, electrolyte decomposition, and complex cathode–electrolyte interphase (CEI) formation, resulting in severe capacity fading of LIBs.[3,5−7] Thus, a suitable cathode with surface modification may trigger the electrochemical performance of the LIBs.

Significant efforts have been dedicated on increasing the energy density of LIBs by developing suitable high-voltage cathode materials such as lithium-rich layered oxide cathodes ($Li_{1+x}M_{1-x}O_2$, M = Ni, Co, and Mn),[3,8] nickel-rich layered oxide cathodes ($LiNi_xCo_yMn_zO_2$ and $LiNi_xCo_yAl_zO_2$ ($x + y + z = 1$),[9] high-voltage polyanionic cathodes (silicates, phosphates, sulfates, etc.),[10−12] and high-voltage spinel oxide cathodes ($LiNi_{0.5}Mn_{1.5}O_4$).[13] Among these cathodes, LNMO offers high

Received: June 17, 2024
Revised: September 20, 2024
Accepted: October 7, 2024
Published: October 16, 2024

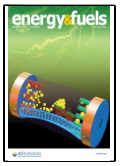

https://doi.org/10.1021/acs.energyfuels.4c02933
Energy Fuels 2024, 38, 21456–21467

Scheme 1. Schematic Representation of Synthesis of LNMO Nanopowders and Preparation of the Composite Cathode via the IECHP Coating on the LNMO Electrode

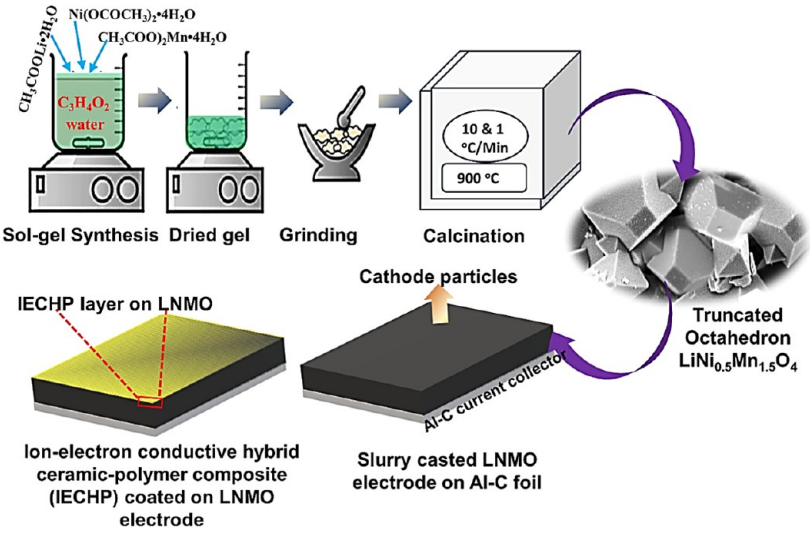

working potential, is easy to synthesize, show good rate performances, is highly economic, and has high thermal stability, making it an appropriate cathode material for LIBs in EV industries.[13,14] In principle, LNMO possesses a higher energy density (650 W h/kg) than $LiCoO_2$ (518 W h/kg) and $LiFePO_4$ (495 W h/kg).[13] Nevertheless, conventional liquid electrolytes (LEs) are not stable with the LNMO cathode under high-voltage conditions (~4.7 V), resulting with electrolyte decomposition, transition metal dissolution, and complex CEI formation, deteriorating the electrochemical cycling performance of LIBs.[3] Many recent efforts have been devoted to overcome the instability of LNMO with LEs, including electrode surface coating, interface engineering,[15] electrolyte modification,[16] and by the use of solid electrolytes (SEs).[17] The formation of cathode−electrolyte interlayers and material deterioration occurs predominantly on the surface of cathode particles.[8,19−22] Surface modification is an effective strategy for improving the interface chemistry and stability of LNMO with conventional LEs without changing the cathode- or electrolyte-active materials, which reduces the direct contact between cathode-active materials and electrolytes, which improves the interface stability.[18] Nonetheless, there is no appropriate particle morphology or surface coating that allows LNMO to meet practical applications with LEs.

SEs are promising materials for LNMO-based cathode materials, but their poor conductivity and complexity hinder commercial implications.[23] Therefore, applying a hybrid SE, such as a ceramic−polymer composite, as a protective layer on an LNMO of suitable morphologies with that of a LE is a possible way to boost the long-term cycle life of LNMO-based LIBs. Following this hypothesis, in this research, we describe a unique approach for preventing direct contact between cathode-active particles and LEs by coating the surface of the truncated octahedron-shaped LNMO electrode with an ion−electron-conductive (ambipolar) hybrid polymer−ceramic−carbon electrolyte (IECHP) via a simple slurry casting method. The IECHP was a composite made up of $Li_{6.25}La_3Zr_2A_{0.25}O_{12}$ (LLZAO) ceramic nanofibers, polyvinylidene fluoride (PVDF), lithium Bis(trifluoromethanesulfonyl)-imide (LITFSI), and carbon. The ionic conductivity and electrochemical stability of a hybrid polymer electrolyte (HPE) were optimized and reported in our previous work.[24] The IECHP-coated truncated octahedron-shaped LNMO demonstrated excellent long-term electrochemical cycling stability, with a capacity retention of 86.11% after 1000 cycles using conventional $LiPF_6$-LE in EC:DMC at 1 C. The postanalysis of focused ion beam scanning electron microscopy (FIB-SEM) and time-of-flight secondary ion mass spectrometry (ToF-SIMS) mapping suggested that the pristine LNMO produces an inactive layer on the cathode surface, reducing ionic transport between the cathode and the electrolyte and increasing the interface resistance. Even after 1000 charge−discharge cycles, the IECHP coating layer remained intact, preventing the direct influence of surface-active cathode particles on LEs and minimizing transitional metal ion dissolution.

2. EXPERIMENTAL SECTION

2.1. Materials. The lithium acetate dihydrate ($CH_3COOLi·2H_2O$, Sigma-Aldrich, 98%), nickel(II) acetate tetrahydrate ($Ni(OCOCH_3)_2·4H_2O$, Sigma-Aldrich, 99.995%), manganese(II) acetate tetrahydrate ($(CH_3COO)_2Mn·4H_2O$, Sigma-Aldrich, 99%), and acrylic acid ($C_3H_4O_2$, Sigma-Aldrich) were used as raw materials for the preparation of LNMO cathode materials. The carbon-coated aluminum foil and conductive carbon black (MSE supplies, USA), Bis(trifluoromethanesulfonimide) lithium salt (LiTFSI) (99.99%, Sigma-Aldrich), glacial acetic acid (Sigma-Aldrich), PVDF-based binder (99.95%, MTI), and (LLZAO) ceramic nanofibers were used for the fabrication of IECHP.

2.2. Preparation of Truncated Octahedron-Shaped LNMO Cathode Materials. The spinel-type truncated octahedron-shaped LNMO cathode materials were synthesized by the polymer-embedded sol−gel process using acrylic acid as a chelating agent with two distinct calcination approaches, as demonstrated in Scheme 1. The stoichiometric amounts of lithium acetate dihydrate, nickel(II) acetate tetrahydrate, and manganese(II) acetate tetrahydrate were dissolved in 200 mL of distilled water and thoroughly mixed to form a uniform solution. The precursor solution was then mixed with 0.13 M acrylic acid and agitated at 95 °C until the formation of a dry gel. Half of the dry precursor gel was directly calcined at 900 °C in an air environment with a rapid heating rate (10 °C/min) and a long calcination duration (10 h) (named as LNMO-A), whereas the other half was calcined at 900 °C with a slow heating rate (1 °C/min) and a short duration (1 h) (named as LNMO-B).

https://doi.org/10.1021/acs.energyfuels.4c02933
Energy Fuels 2024, 38, 21456−21467

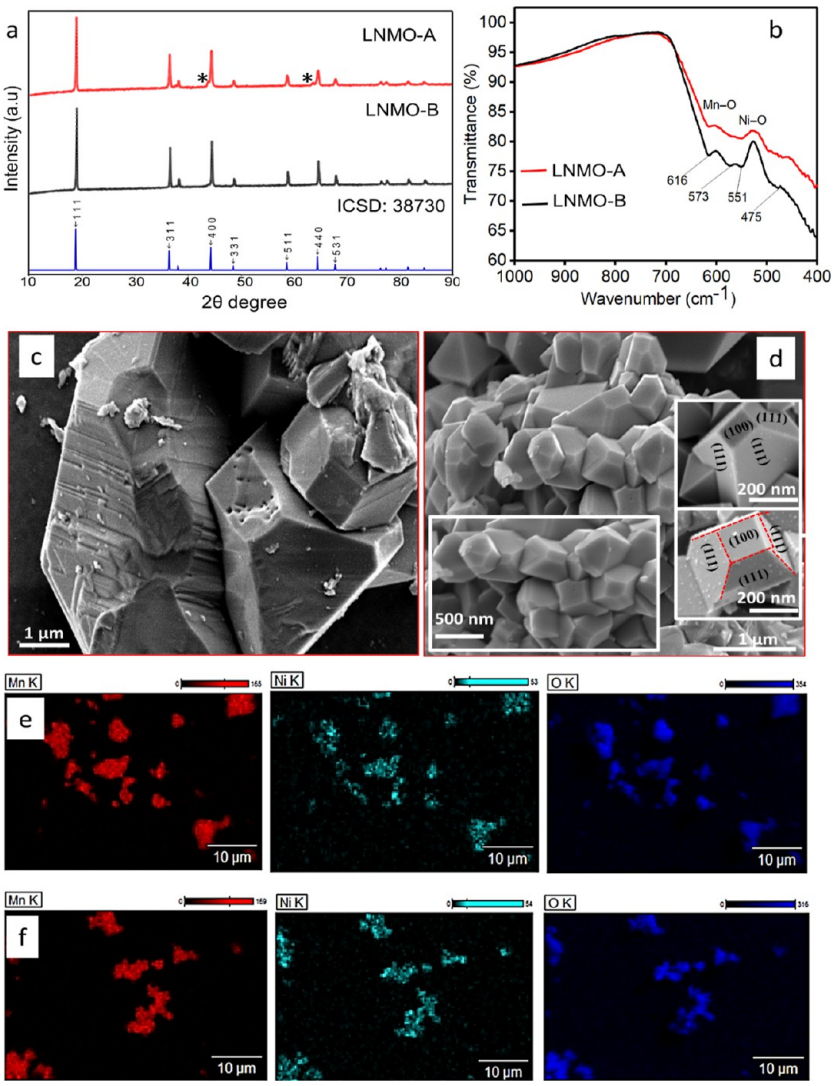

Figure 1. (a) XRD pattern, (b) FTIR spectra, (c,d) FE-SEM micrographs, and (e,f) EDS mapping of LNMO-A and LNMO-B.

2.3. Preparation of the Electrode and the Coating of IECHP on LNMO. The LNMO-A and LNMO-B electrodes were prepared by mixing the as-synthesized LNMO (A/B) (85%), PVDF binder (10%), and carbon additive Super P carbon (5%) into *N*-methyl-2-pyrrolidone (NMP) and stirring for 12 h to form a homogeneous slurry. The LNMO slurry was slot-die-coated on carbon-coated Al foil and heated in a vacuum oven at 120 °C for 12 h to evaporate the solvent. IECHP was prepared by using the optimized composition of the LLZAO ceramic nanofiber-polymer HPE and carbon. The ionic conductivity and electrochemical stability of the HPE were reported in our previous report.[24] The high Li-ion conducting HPE was chosen (PVDF/LiTFSI/LLZAO: 60/25/15 wt %) for the preparation of IECHP composite. The 60 wt % PVDF, 25 wt % LITSFI, 15 wt % LLZAO ceramic nanofibers, and 5 wt % super P carbon powder with respect to the total weight percentage of the HPE were dispersed in NMP and agitated for 24 h to form a homogeneous slurry. The IECHP slurry was coated on the optimized LNMO-B electrode (IECHP-LNMO-B) using slot-die coating and heated in a vacuum oven at 120 °C for 12 h to remove the solvent (Scheme 1). The mass loading of the IECHP-LNMO-B cathode was 3.306 mg. The IECHP-coated LNMO-B cathode was stored in a glovebox with oxygen and water levels <1 ppm.

2.4. Characterization. The X-ray diffraction (XRD) measurement was carried out by a powder diffractometer (PANalytical XPert Pro) using Cu Kα radiation (λ = 1.54187 Å) in the 2θ range of 10–90°. The vibrations from different functional groups in LNMO were determined by FTIR analysis (PerkinElmer). The morphology and elemental mapping of LNMO (A and B) powder were examined by using field emission scanning electron microscopy (FE-SEM) (Zeiss Leo 1530). For the evaluation of cross-sectional morphology and chemical composition of the LNMO electrode and IECHP-coated LNMO, FIB cross sections were prepared in a Zeiss Crossbeam 550 SEM instrument (Carl Zeiss Microscopy GmbH, Oberkochen, Germany), which is equipped with an IonSculptor-Ga-FIB and investigated with an Oxford Ultim Max (170 series) energy-dispersive spectroscopy detector. The samples were mounted onto a 54-angle pretilted holder, and a probe current of 65 nA and 30 kV are employed for depth-specific preliminary cutting with a trapezoid-shaped trench. For polishing of the cross section, a probe current of 15 nA and 30 kV were employed with a thin rectangle-shaped trench. To project the mechanism of cell breakdown in LNMO cathodes after long-term cycling, ToF-SIMS was performed. The analysis was carried out directly inside the Zeiss Crossbeam 550 SEM instrument using a retractable ToF-SIMS detector (cTOF, tofwerk AG, Thun, Switzerland), without being transferred to a different environment after FIB processing.

2.5. Coin Cell Assembly and Electrochemical Testing. The LNMO electrodes, Celgard-2400 separator, and lithium foil (200 μm) were punched into 13, 16, and 14 mm diameters, respectively. All the electrodes were dried at 80 °C in a high-vacuum oven for 12 h before assembling the coin cells. The CR2032 type coin cells were fabricated by sandwiching the cathode, separator, and lithium with LE $LiPF_6$ (1

https://doi.org/10.1021/acs.energyfuels.4c02933
Energy Fuels 2024, 38, 21456–21467

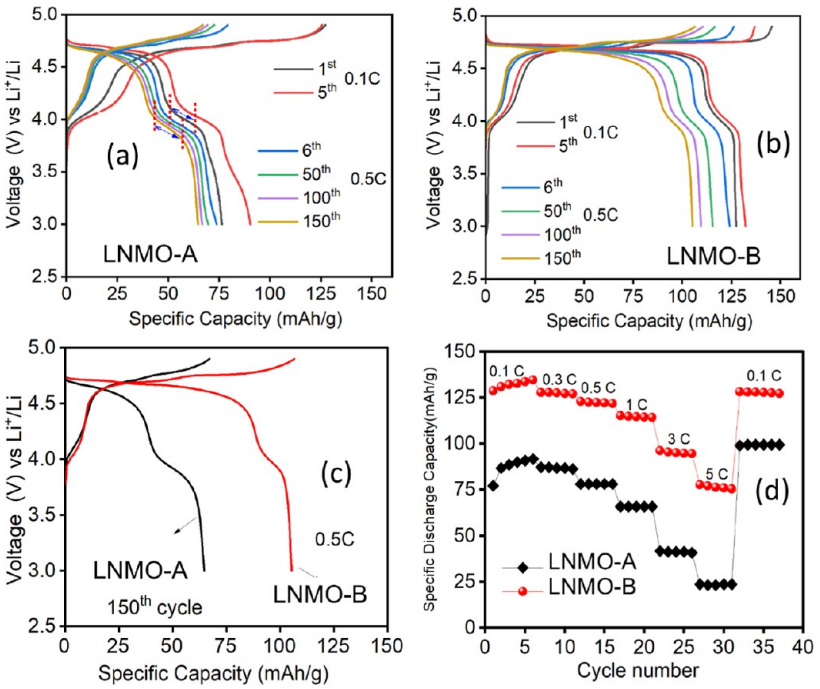

Figure 2. (a,b) Charge−discharge curves, (c) comparison of charge−discharge curves after 150th cycles at 0.5 C rate, and (d) rate performance of LNMO-A and LNMO-B.

m) in EC/DMC, 1:1 v/v (70 μL) (Sigma-Aldrich). All of the cells were fabricated inside the glovebox with oxygen and water contents ≤0.1 ppm. The battery performance of the LNMO (A and B) and IECHP-coated LNMO were tested using a Neware battery tester (CT-4008Tn-5 V50 mA). All the cells were charged−discharged by the constant current (CC) mode at 0.1 C, 0.5, and 1C rates at 25 °C within the voltage range of 3−4.9 V. The rate performance of the samples was tested by applying different current rates such as 0.1, 0.3, 0.5, 1, 3, 5, and 0.1C, and the cells were cycled 5 times for each current rate. Electrochemical impedance spectroscopy (EIS) was used to assess the lithium-ion diffusion and charge-transfer resistance of the cells before and after cycling at frequencies ranging from 100 mHz to 100 kHz.

3. RESULTS AND DISCUSSION

3.1. Microstructural and Electrochemical Optimization of the LNMO Cathode. The calcination temperature and heating rate are critical parameters in the synthesis of high-performance LNMO materials. The structural and electrochemical performance of LNMO is improved by altering the calcination procedure. Numerous studies have focused on the synthesis of LNMO at various calcination temperatures in order to get the pure phase spinel LNMO.[25,26] The heating rate of the sample plays an important role in tailoring the surface morphology and in controlling nucleation and uniform particle growth. LNMO-A was calcined at 900 °C with a rapid heating rate (10 °C/min) and a long calcination duration (10 h), while LNMO-B was calcined at 900 °C with a slow heating rate (1 °C/min) and a short duration (1 h). Figure 1a represents the powder XRD patterns of the LNMO-A and LNMO-B cathodes, the Rietveld refined XRD patterns are depicted in Figure S1, and refinement results and lattice parameters are tabulated in Table S1. Both samples exhibit the same cubic spinel structure with the space group $Fd\bar{3}m$.[27,28] The lattice parameters of LNMO-A and LNMO-B are a = 8.178(5) Å and a = 8.168(3) Å, respectively. The high a value at a rapid heating rate is owing to the greater ionic radius of Mn^{3+} (0.645 Å) than Mn^{4+} (0.53 Å).[29] LNMO-B calcined at a slow heating rate has a lower unit cell volume (544.99 Å^3) compared to LNMO-A (547.04 Å^3) calcined at a rapid heating rate (10 °C/min). The rise in the lattice parameters of LNMO-A due to the oxygen and nickel deficiencies led to the formation of the NiO impurity phase (12.7%), which is also evidenced by the XRD pattern (small diffraction peaks at 43.2 and 63.02° highlighted as * in the XRD pattern), whereas LNMO-B has no impurity phases. The presence of characteristic metal oxide functional groups in LNMO-A and LNMO-B is confirmed by FTIR spectra, as illustrated in Figure 1b. The Mn−O and Ni−O vibrational modes are relatively prominent when the heating rate is limited to 1 °C/min (LNMO-B); however, all vibrational modes are identical to LNMO-A. The surface morphology of the cathode has a direct influence on electrochemical performance due to the surface reaction between the active cathode particles and the electrolyte. When LNMO-A is calcined at 10 °C/min, it has an inhomogeneous shape and high particle size (Figure 1c.). Interestingly, LNMO-B calcined at a low heating rate exhibits homogeneous morphology with truncated octahedron-shaped particles.[30] The low heating rate prevents aberrant particle growth and preserves homogeneous particle sizes of 400−500 nm (Figure 1d). The truncated octahedron-shaped LNMO particles have been identified as a suitable microstructure for achieving superior electrochemical performance.[30] There are numerous techniques for synthesizing LNMO with an octahedron shape,[31] but in this study, the truncated octahedron-shaped LNMO was synthesized using a simple approach by altering the heating rate and duration of the calcination temperature. A truncated octahedron LNMO with {100} facet is more effective for lithium-ion transport than the typical octahedral spinel LNMO.[6] The presence of expected elements (Ni, Mn, and O) is ensured by EDS mapping as shown in Figure 1e,f.

https://doi.org/10.1021/acs.energyfuels.4c02933
Energy Fuels 2024, 38, 21456−21467

The electrochemical performance of LNMO-A and LNMO-B was tested by assembling the coin cells (Li|LiPF$_6$-EC:DMC|LNMO-A and Li|LiPF$_6$-EC:DMC|LNMO-B), and the cells were charged and discharged at 0.1C for 5 cycles for the facile Li-ion movement during cycling; then, the current was increased to 0.5C for 150 cycles with the voltage range of 3.0−4.9 V. The charge−discharge profiles for selected cycles are depicted in Figure 2a,b. LNMO-A provides an initial charge and discharge capacity of 127 and 76 mA h g^{-1}, respectively, with a Coulombic efficiency (CE) of 59.84%. After 5 cycles, the cells have a charge and discharge capacity of 125 and 90 mA h g^{-1}, respectively, with a CE of ∼72% at 0.1C. LNMO-B displayed initial charge−discharge capacities of 148 and 125 mA h g^{-1}, respectively, with a CE of 84.45%, which is higher than that of LNMO-A. The CE reached 97.03% after the fifth cycle. The LNMO-A cathode exhibited two voltage plateaus during charge and discharge (Figure 2a), one at 4.65 V due to the redox process of Ni^{2+}/Ni^{3+} and Ni^{3+}/Ni^{4+} and the other at 4.06 V due to the redox reactions of Mn^{3+}/Mn^{4+}.[32] These voltage plateaus are slightly shifted (4.57 and 4.01 V) and possess gradual slope with a loss of clear plateau feature over subsequent cycles. This shift can be attributed to the structural changes or distortions in the LNMO lattice induced over the repeated cycling and different lithium-ion occupancy states in the spinel structure caused by the NiO impurity phase. The redox process of Mn^{3+}/Mn^{4+} continually produces Mn^{2+}, which is highly soluble in LEs, thereby decreasing the capacity.[33] In addition, prolonged cycling at high voltages of LNMO-A with irregular morphology and impurity phase leads to an irreversible structural change, which in turn reduces the capacity retention of the LNMO-A cathode. LNMO-B shows a well-defined voltage profile with two distinct voltage profiles at 4.74 and 4.1 V vs Li/Li$^+$ (Figure 2b), which are found to be negligible shifts or loss of plateaus nature over the cycling attributed to the good electrochemical redox reactions and good structural stability. The voltage plateau owing to Ni^{2+}/Ni^{4+} of LNMO-A decreases with a rise in the charge−discharge cycles, while the plateau due to Mn^{3+}/Mn^{4+} slightly raised after 150 cycles (marked in Figure 2a), LNMO-B displays negligible variations in the voltage plateaus. The capacity of LNMO-A and LNMO-B due to the redox reaction of Mn^{3+}/Mn^{4+} was determined to be 27% and 13%, respectively.

As shown in Figure 2d, the rate performance of LNMO-A and LNMO-B was examined by charging and discharging the cells at various C rates (0.1, 0.3, 5, 1, 3, 5, and 0.1 C) for 5 cycles. LNMO-B demonstrated higher discharge capacity for all current rates, indicating that truncated octahedron-shaped particles are appropriate for efficient lithium transfer. The discharge capacity of LNMO-B is 134, 128, 121, 115, 96, 77, and 129 mA h g^{-1} at 0.1, 0.3,0.5, 1, 3, 5, and 0.1 C, respectively, indicating that LNMO-B has a better rate capability than LNMO-A. Furthermore, LNMO-B exhibits 129 mA h g^{-1} when the current rate is further reduced to 0.1 C, indicating that LNMO-B has a high tolerance for fast charge−discharge cycles. Figure 3a and c depict the cycling performance of LNMO-A and LNMO-B at 0.5 C for 150 cycles and at 1 C for 200 cycles. LNMO-B revealed a discharge capacity of 105 mA h g^{-1} after 150 cycles at 0.5 C and 98 mA h g^{-1} after 200 cycles at 1 C. The high heating rate, large particle size, and NiO impurity have an impact on the cycling performance of the LNMO-A sample; after 150 and 200 cycles, it delivers 66 and 56 mA h g^{-1} at 0.5 and 1 C, respectively

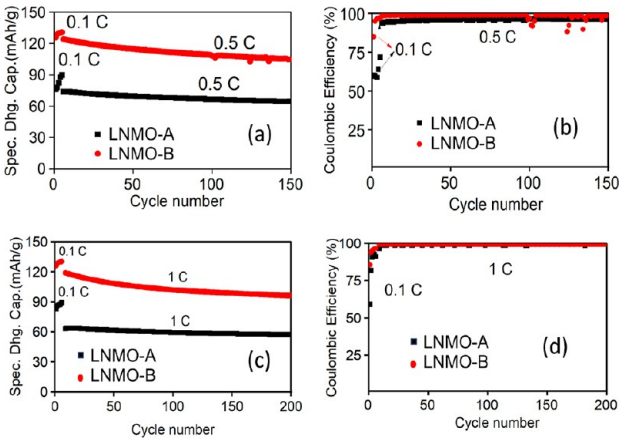

Figure 3. (a,c) Cycling stability and (b,d) CE of LNMO-A and LNMO-B cells at 0.5 and 1 C rates.

(Figure 3a,c). NiO did not participate in the electrochemical reactions similar to LNMO, so it effectively diluted the amount of active material that can contribute to cell performance. Moreover, the NiO impurity could accelerate the degradation of the LNMO cathode material during cycling by altering the stability of the cubic spinel structure of LNMO, leading to a low capacity and reduced cycle life. The LNMO-B cathode provides a higher CE than LNMO-A as shown in Figure 3b,d.

The truncated octahedron shape offers larger surface area compared to irregular microparticle/spherical or cuboidal particle distributions. The increase in the surface area enhances the contact between the cathode material and the electrolyte, improving the overall electrochemical reactivity and ion-exchange efficiency. The unique geometry reduces the average Li-ion hoping distance within the particle.[34] Shorter diffusion paths help in minimizing the resistance during lithium-ion intercalation and deintercalation processes, leading to a better rate capability and faster charge/discharge kinetics. The truncated octahedron shape can lead to a more uniform stress distribution during cycling compared to other shapes. The truncated octahedron morphology can create more efficient pathways for lithium-ion movement within the material and minimizing resistance to lithium-ion transport through the crystal structure.[6] This can help in maintaining structural integrity and reducing mechanical degradation, which is crucial for long-term cycle stability. The results demonstrated that LNMO-B has a homogeneous morphology with truncated octahedron-shaped particles without any impurity phases facilitated better electrochemical performance than LNMO-A.

3.2. Electrochemical Performance of the Ion−Electron-Conductive IECHP-Coated LNMO Cathode. LNMO-B has a truncated octahedron morphology with nanoparticles (400−500 nm), which exposes more active surface area for lithium-ion intercalation and deintercalation. This results in a higher specific capacity since more lithium ions can participate in the charge/discharge process. The well-defined facets and uniform morphology of truncated octahedrons often facilitate better lithium-ion diffusion, which enhances the rate performance. A smooth and regular surface can reduce the diffusion pathway and improve the electrochemical kinetics.[34] However, the higher surface area also means increased exposure to side reactions with LE decomposition, which can lead to faster capacity fading over cycling. Moreover, the increased surface area might enhance structural degradation due to repeated

https://doi.org/10.1021/acs.energyfuels.4c02933
Energy Fuels 2024, 38, 21456−21467

lithium insertion/extraction cycles, causing a rapid decline in capacity over time. Although the LNMO-B cathode materials exhibited acceptable electrochemical performances, their cycling life is insufficient due to the electrochemical instability of the LE when working at a high voltage. Thus, surface modification is required for the LNMO cathode to achieve a long-term cycle life. Several surface modification techniques have been attempted,[7,33] but the previous approaches are complex and nonscalable. Herein, we have developed a unique technique to solve the interfacial degradation problems of high-voltage LNMO cathode material, which is easily accessible and scalable. After optimizing the truncated octahedron LNMO synthesis, the best-performing truncated octahedron-shaped LNMO-B cathode was preferred for further surface modification with IECHP on the surface of the cathode-active particles using a simple slot-die coating process. Figure 4a and c shows SEM micrographs of LNMO-B- and

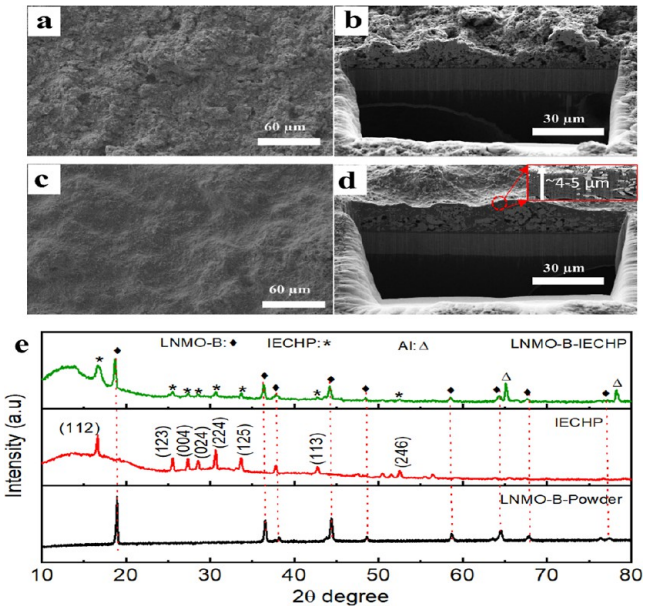

Figure 4. Surface and cross-sectional FIB-SEM micrographs; (a,b) LNMO-B electrode; (c,d) IECHP-coated LNMO-B electrode; and (e) XRD pattern of LNMO-B powder, IECHP composites, and IECHP-coated LNMO-B electrode.

IECHP-coated LNMO-B electrodes' surface before cycling, demonstrating that the IECHP was evenly coated on the surface of the cathode electrode. The cross-sectional FIB-SEM is an advanced technique to determine the coating layer of the IECHP. As shown in Figure 4b,d, a thin layer of IECHP (~4–5 μm) is coated on the LNMO-B electrode (Figure S2). Additionally, through side-view FIB-SEM images, it can be demonstrated that the degree of surface roughness at the top of the electrode is lower in the electrode treated with IECHP coating compared to the untreated LNMO electrode.

The diffraction peaks of IECHP-coated LNMO-B are similar to those of LNMO-B powder (Figure 4e), indicating that the SE-based IECHP coating has no effect on the crystal structure of the cathode-active material.

In addition to the typical diffraction peaks of LNMO, a few minor peaks at 16.2, 25, 26, 30, and 53° are attributed to LLZAO ceramic nanofibers[24] that were included in the IECHP composite, and *hkl* planes are indexed in the XRD pattern. The XRD pattern confirms the existence of the IECHP on LNMO-B. Figure 5 depicts the cross-sectional and surface (Figure S3a) EDS mappings of LNMO-B and IECHP-coated LNMO-B electrodes. The LNMO-B electrode contains Mn, Ni, and O from LNMO, as well as C and F from the carbon additive and PVDF binder; Al is a current collector. The presence of IECHP is confirmed by EDS mapping, as shown in Figures 5b and S3b; the predicted elements are found to be Mn, Ni, O, Al, C, F, Zr, and La; the elements La, Zr, O, F, and C appear from the IECHP composite (LLZAO/PVDF/LITFSI/carbon).

The morphological, structural, and elemental investigations reveal that the IECHP is uniformly coated on the LNMO-B electrode. The long-term cycle life of LNMO-B- and IECHP-protected LNMO-B cathode was performed at 1 C rate over 1000 charge−discharge cycles at 25 °C, as shown in Figure 6a. The LNMO-B cathode has a discharge capacity of 69 mA h g^{-1} after 980 charge−discharge cycles with a capacity retention of 57%. Despite its short cycle life, the LNMO-B cell exhibits considerable disparity in discharge capacity after 980 cycles, indicating cell failure and electrolyte decomposition (dotted circle in Figure 6a). The IECHP-LNMO-B cell had a slightly lower initial capacity than LNMO-B during cell formation at 0.1 C for 5 cycles, which might be attributed to the growth of the CEI and the creation of Li-ion diffusion pathways between the cathode and the LE via the IECHP layer. As a result, the IECHP-coated LNMO-B cathode had a discharge capacity of 93 mA h g^{-1} after 1000 cycles and a capacity retention of 86.11%, which is significantly higher than that of the pristine LNMO-B. Furthermore, the IECHP-coated LNMO-B displayed negligible fading (capacity retention ~98%) even after 250 cycles at 1 C rate, as shown in Figure 6b, which is superior in its electrochemical performance when compared to the previous studies on LNMO cathodes.[33−41] The findings show that the unique ceramic nanofiber−polymer composite coating provided outstanding CEI compatibility at high-voltage operation. The CEI coating enabled the use of conventional LEs for high-voltage LNMO cathode materials. The IECHP coating prevents the dissolution of the metal ion Mn^{2+} by protecting the direct contact between the LE and the surface of cathode-active particles. In addition, when LiTFSI is added to IECHP, it enhances the lithium ion conductivity within the composite, potentially reducing polarization during the first charge/discharge cycle. This can lead to a higher initial CE, as more lithium ions are effectively cycled without being trapped in side reactions.

The dQ/dV vs V curves (Figure 6c,d) demonstrate the redox reaction mechanism in LNMO cathodes. Two prominent oxidation peaks at 4.7−4.77 V and reduction peaks between 4.65 and 4.69 V depict the redox reaction of Ni^{2+}/Ni^{4+} during charge−discharge cycles at 1C rate. LNMO-B shows a pair of redox peaks at 4.707/4.65 and 4.776/4.701 V attributed to the redox reactions of Ni^{2+}/Ni^{3+} and Ni^{3+}/Ni^{4+} (Figure 6c), respectively, after 50 cycles, while the oxidation peaks shifted to a higher potential (4.728 and 4.801 V), and the reduction peaks shifted to a lower potential (4.62 and 4.69 V) after 1000 cycles. In addition to peak shifts, the differential capacity decreased significantly, reducing the electrochemical reactions. The IECHP-LNMO-B cell exhibits redox peaks at 4.701/4.651 and 4.765/4.695 V after 50 cycles, which are comparable to redox peaks obtained at 4.709/4.65 and 4.77/4.694 V after 1000 charge−discharge cycles (Figure 6d). Intriguingly, IECHP-coated LNMO-B exhibits a negligible shift in redox peaks and in differential capacity loss even after 1000 cycles. The redox peak separation potential (ΔV_p)

https://doi.org/10.1021/acs.energyfuels.4c02933
Energy Fuels 2024, 38, 21456−21467

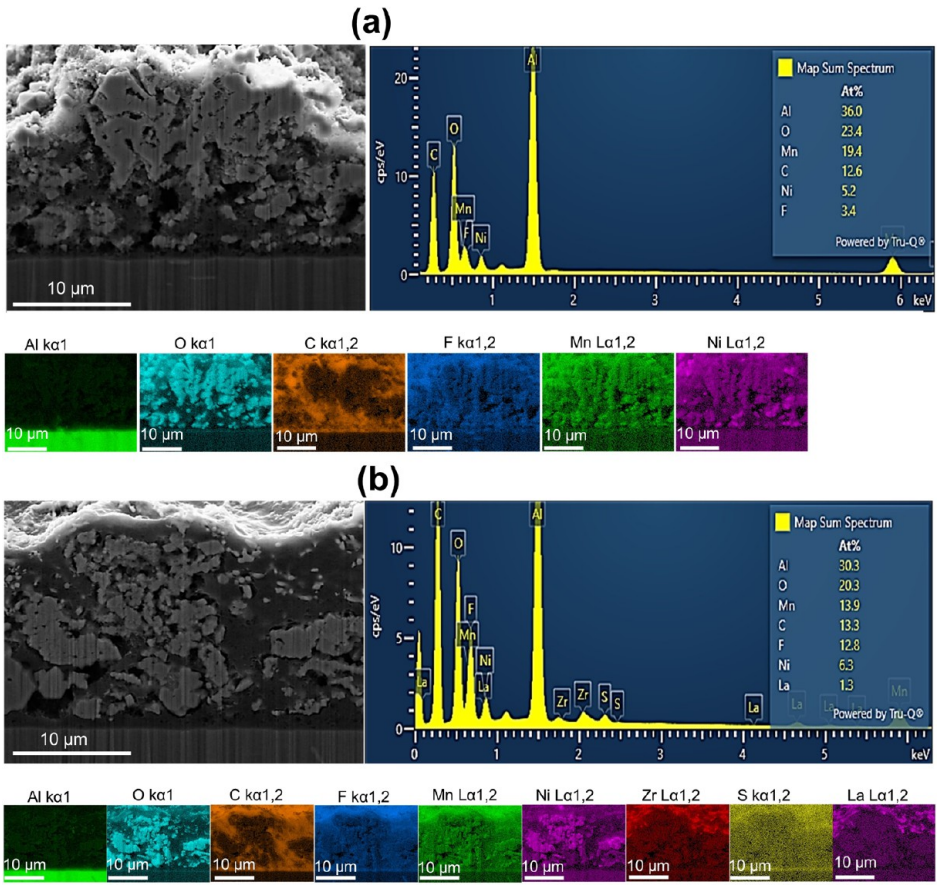

Figure 5. Cross-sectional FIB-SEM EDS mapping of the as-prepared (a) LNMO-B and (b) IECHP-coated LNMO-B electrodes.

between Ni^{2+}/Ni^{3+} and Ni^{3+}/Ni^{4+} redox couples determines the phase change of spinel LNMO, where ΔV_p >50 mV indicating a disordered phase and ΔV_p <30 mV indicating an ordered phase of the LNMO cathode.[37,42] After 50 cycles, ICHEP-coated LNMO-B exhibits redox ΔVp values of 61 and 44 mV, which are nearly identical after 1000 cycles (64 and 44 mV). LNMO-B exhibits redox ΔV_p values of 69 and 51 mV after 50 cycles, which increased to 73 and 70 mV after 1000 charge−discharge cycles. Both samples had disordered phases, but the ΔV_p values of IECHP-LNMO-B remained stable even after 1000 cycles, indicating that the ceramic−polymer coating prevents phase shifts during charge−discharge cycles and provides superior electrochemical reversibility. The LNMO-B cell exhibits substantial variations in ΔV_p values during long-term cycling, indicating chaotic phase changes during charge−discharge cycles and severe capacity fading. The incorporation of LLZO ceramic nanofibers into the IECHP composite improved the ionic conductivity of the polymer−ceramic composite, facilitating faster lithium-ion transport to and from the LNMO-B cathode during charge/discharge cycles. LLZO is chemically and electrochemically stable, which protected the LNMO cathode from side reactions with the LE. This stabilization is crucial because LNMO cathodes operate at high potentials (4.7 V vs Li/Li^+), where the degradation of LEs can occur. Also, LLZO ceramic nanofibers provide mechanical reinforcement to the polymer matrix, making the composite coating more resistant to cracking or degradation during cycling of the LNMO cathodes. Moreover, LLZO has the potential to suppress lithium dendrite growth, a common issue in LIBs that can lead to short circuits and poor cycling performance. The physical barrier properties of LLZO combined with its high ionic conductivity help prevent dendrites from reaching the LNMO cathode, improving safety and cycle life. This synergy between the polymer matrix, LLZO nanofibers, and LNMO results in a cathode that can deliver excellent long-term cycling stability.

3.3. Failure Mechanism of Cells during Cycling—Post Analysis of Cycled Cells. EIS has been employed to assess the charge-transfer characteristics of the cells before and after long-term cycling, which is depicted in Figure 6e,f. All Nyquist plots were theoretically fitted by EC-Lab software with an equivalent circuit model (inset picture in Figure 6e,f), where R_b is the electrolyte resistance, CPE is the constant phase element, and R_{ct} and R_{it} are the charge-transfer and interface resistance, respectively. The fitted parameters are given in Table S2. The Nyquist plots of LNMO-B and IECHP-coated LNMO-B before cycling (after cell formation) show a high-frequency semicircle and a low-frequency spike, which are due to charge-transfer resistance and Li-ion diffusion.[42] Before cycling, IECHP-coated LNMO-B cells illustrate a lower charge-transfer resistance (229 Ω) compared to LNMO-B cells (273 Ω). The IECHP coating can smoothen the surface of the LNMO-B particles, reducing surface roughness and irregularities. A smoother surface promotes better contact with the electrolyte and reduces the resistance associated with surface defects or irregularities. The IECHP coating can provide additional mechanical support to the LNMO-B particles, reducing structural degradation and maintaining a stable electrode structure. During initial cycling, particles can deform or change shape, affecting charge transfer. The IECHP

https://doi.org/10.1021/acs.energyfuels.4c02933
Energy Fuels 2024, 38, 21456−21467

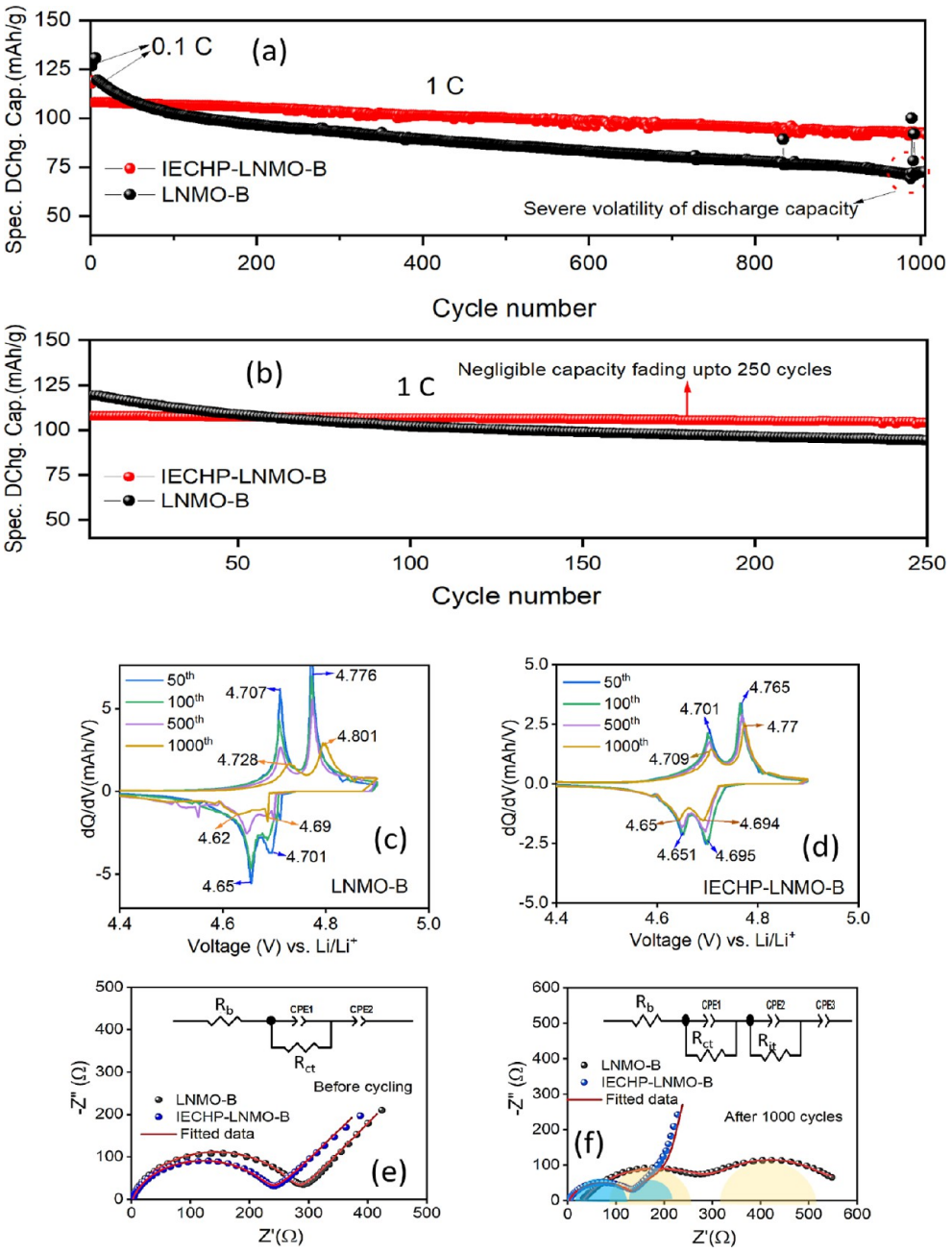

Figure 6. (a,b) Long-term cycling performance at 1C rate, (c,d) dQ/dV vs voltage curves, and (e,f) EIS spectra of LNMO-B and IECHP-LNMO-B cells.

coating can help in minimizing such deformations, ensuring consistent charge-transfer characteristics. After 1000 cycles, the IECHP-LNMO-B cell exhibits a high-frequency semicircle and a small low-frequency semicircle, whereas LNMO-B shows relatively two big semicircles associated with charge-transfer resistance and interfacial resistance (Figure 6f). The IECHP-LNMO-B cell has a charge-transfer resistance of 135 Ω and an interfacial resistance of 65 Ω after 1000 cycles, which is lower than those of the LNMO-B electrode (272 and 277 Ω). Prolonged cycling at high voltage can degrade the electrolyte, increase the CEI, and induce phase transitions or structural transformations in LNMO-B, such as the formation of undesired phases (e.g., Li_xO, and Li_xNi_yO),[29] which can disrupt the crystal lattice and increase charge-transfer resistance.[38,39] In addition, repeated expansion and contraction during cycling can cause mechanical stress and lead to particle cracking, which can hinder effective electron and ion transport. Over time, the loss of the active material due to degradation or dissolution reduces the effective surface area available for electrochemical reactions, leading to an increased resistance. Also, long-term cycling can degrade the conductive pathways within the electrode material, either by physical damage or by the loss of conductive additives, leading to increased charge-transfer resistance of LNMO-B. However, the IECHP coating on LNMO-B significantly addressed the aforementioned issues and demonstrated good long-term cycling performance. The IECHP coating on LNMO mitigates the direct contact between electrolyte and cathode particles, preventing the oxidative degradation of the electrolyte and the persistent rise of the CEI during cycling. The electronically conductive

https://doi.org/10.1021/acs.energyfuels.4c02933
Energy Fuels 2024, 38, 21456−21467

component in IECHP (e.g., conductive carbon) improves the electron-transfer pathways. This enhanced electron mobility decreases R_{ct} by facilitating faster electron flow during redox reactions at the electrode interface. The ion-conducting polymer−LLZO ceramic composite in the IECHP ensures efficient ion transport. In electrochemical systems, fast ion transport can enhance the rate of charge-transfer reactions, further reducing R_{ct}. The ionic conductivity of the polymer−ceramic composite in the IECHP ensures that ions can move freely across the interface between the cathode coating and the electrolyte. This reduces the buildup of charge at the interface, lowering interfacial resistance. As a result, the unique IECHP coating greatly lowers the interfacial impedance of the LNMO-B sample, which in turn improves the electrochemical cycling efficiency of the sample.

The mechanism of high interfacial impedance and rapid cell failure following long-term cycling of the LNMO cathode has not been thoroughly explored. FIB-SEM and ToF-SIMS are advanced techniques for predicting the undesirable layer formation and the cell failure mechanism of LNMO cathodes after prolonged cycling. The FIB-SEM micrographs of cycled LNMO-B (Figure 7a) indicate a disrupted electrode surface

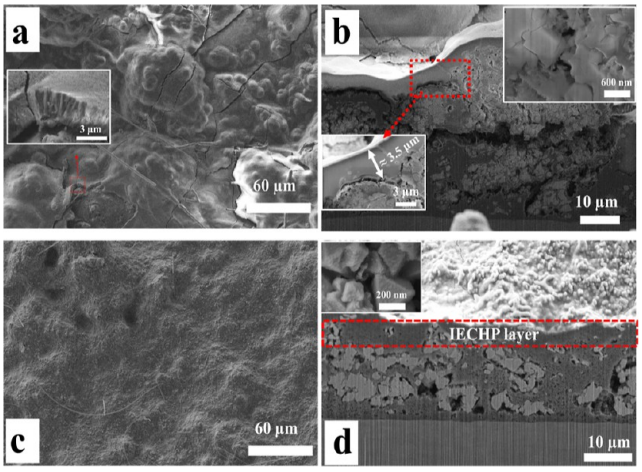

Figure 7. Top surface and cross-sectional FIB-SEM micrographs of (a,b) LNMO-B and (c,d) IECHP-coated LNMO-B cathode after 1000 cycles.

morphology compared to the as-prepared electrode (Figure 4a). After 1000 cycles, the electrode deteriorated, and a thick layer appeared on its surface. The cross-sectional FIB-SEM micrograph clearly shows that the LNMO-B cathode is delaminated, with a thick layer forming on the electrode, as illustrated in Figures 7b and S4a). The thick layer formation on the LNMO-B cathode is attributed to the electrolyte decomposition at the electrode interface, which develops abnormal growth of a layer with a thickness of ∼3−3.5 μm (inset picture of Figure 7b).[43,44] This hinders Li transfer between the cathode and the electrolyte, leading to severe capacity fading and cell failure. Interestingly, the surface morphology of the IECHP-coated LNMO-B electrode before and after 1000 cycles seems comparable (Figures 4c and 7c). As observed in Figure 7d, the flatness of the IECHP-coated LNMO-B electrode surface, which was evident before cycling, could still be confirmed after cycling. In contrast, the uncoated LNMO-B electrode exhibits an uneven thickness on its surface (Figure 7b). Cross-sectional FIB-SEM micrographs show that the IECHP coating layer remained intact and did not crack during the charge−discharge cycles (Figures 7d and S4b). The cross-sectional EDS mapping of the electrodes after 1000 cycles (Figure S5) revealed the presence of anticipated elements in the LNMO-B and IECHP coating layer.

It is noteworthy that the ICHEP coating considerably improves the cathode−electrolyte interface and inhibits transition metal ion dissolution. The distribution of Li on the electrode surface was mapped using ToF-SIMS, as shown in Figure 8a−d. Before cycling, lithium was evenly distributed on the surfaces of both electrodes. After 1000 cycles, there is a lack of lithium on the surface of the LNMO-B electrode, whereas Li ions are evenly distributed on the IECHP-LNMO-B electrode (Figure 8d). Figure 8e−h shows the cross-sectional ToF-SIMS mapping of the electrodes before and after 1000 cycles. It was envisaged that the occurrence of a slightly thick layer after cycling of LNMO-B would hinder lithium-ion diffusion from the cathode to the electrolyte, resulting in significant capacity fading with the LE. Figure 8f depicts the accumulation of lithium from the cathode at the bottom of the inactive layer. The growth of an inactive layer on uncoated LNMO-B is the primary cause of severe capacity fading and cell failure. The cross-sectional TOF-SIMS mapping of IECHP-coated LNMO-B before and after 1000 cycles is similar (Figure 8g,h).

As a result, the simple and distinctive IECHP coating effectively prevents the formation of a blocking layer on the cathode surface during high-voltage operation. The IECHP shortens the diffusion of lithium ions between the cathode and the electrolyte, resulting in a remarkable cycle life for the IECHP-LNMO-B cell.

4. CONCLUSIONS

The truncated octahedron-shaped LNMO cathode materials have been prepared by using the sol−gel technique at different heating approaches. LNMO-B calcined at 900 °C with a slow heating rate (1 °C/min) for short duration (1 h) outperformed than the sample prepared with fast (10 °C/min) heating (LNMO-A) in their electrochemical performance. A unique composite IECHP was developed and coated on the optimized LNMO-B electrode by using a simple slot-die coating process for further improvements of interfacial chemistry. The IECHP-coated LNMO-B delivered a discharge capacity of ∼93 mA h g^{-1} after 1000 cycles with a capacity retention of ∼90% which is superior than that of the uncoated LNMO-B cathode (a discharge capacity of ∼69 mA h g^{-1} after 980 cycles with a capacity retention of 57%) at 1C rate (25 °C). Furthermore, the IECHP-coated LNMO-B exhibited negligible capacity fading even after 250 cycles at 1 C. The mechanism of high interfacial impedance, capacity loss, and cell failure following the long-term cycling of an LNMO-B cathode was investigated using FIB-SEM and ToF-SIMS. It was projected that the formation of an inactive thick layer on the surface of uncoated LNMO-B would hinder lithium-ion transport from the cathode to the electrolyte, resulting in severe capacity fading with the LE. However, the IECHP coating on the LNMO-B electrode provides a superior cathode−electrolyte contact, resulting in an outstanding long-term cycle life, facilitating the use of conventional LEs for high-voltage LNMO cathode materials with trivial capacity fading.

https://doi.org/10.1021/acs.energyfuels.4c02933
Energy Fuels 2024, 38, 21456−21467

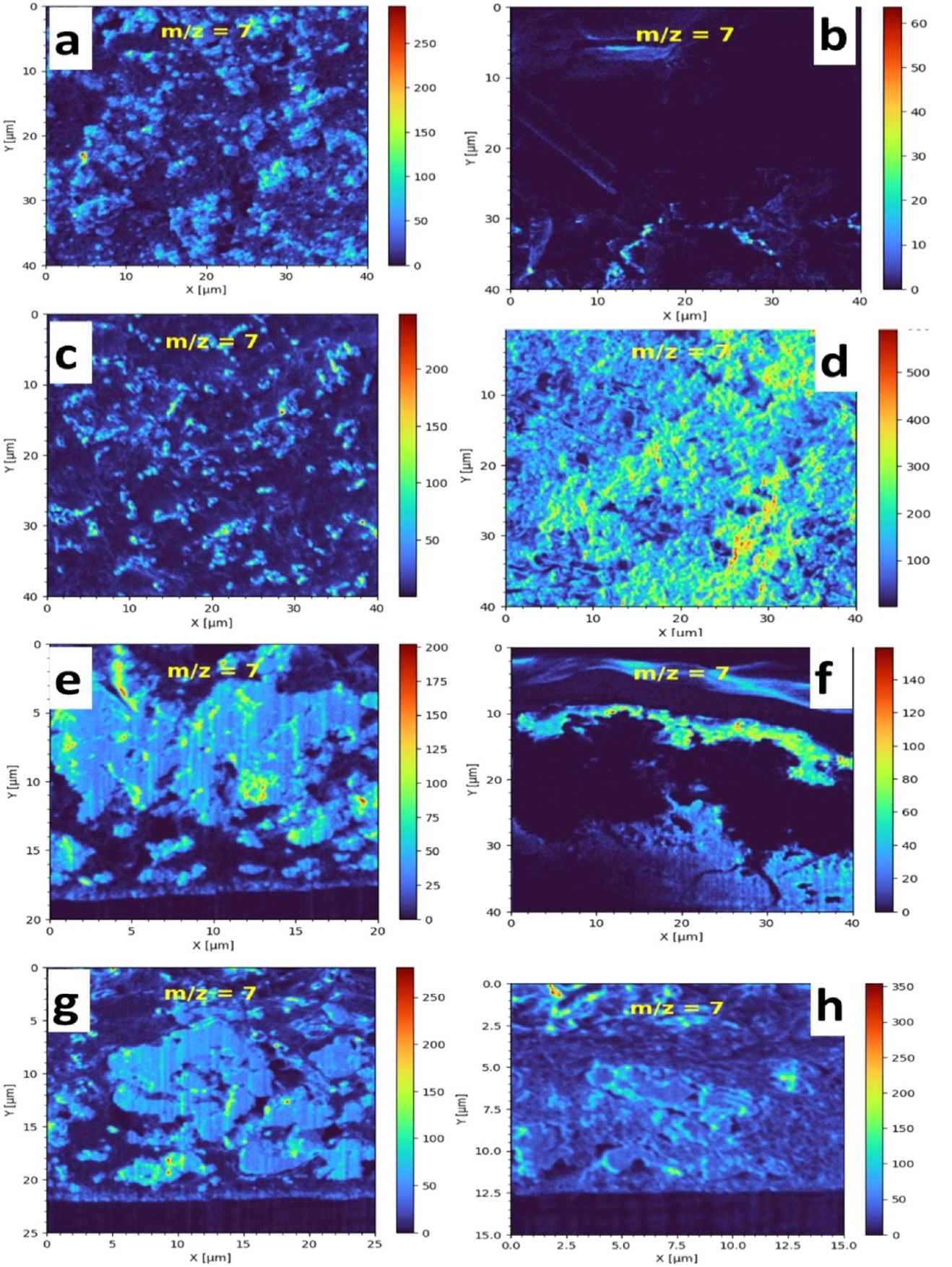

Figure 8. Surface TOF-SIMS mapping of LNMO-B (a) before and (b) after 1000 cycles and IECHP-coated LNMO-B (c) before and (d) after 1000 cycles and cross-sectional TOF-SIMS of LNMO-B (e) before and (f) after 1000 cycles and IECHP-coated LNMO-B (g) before and (h) after 1000 cycles.

https://doi.org/10.1021/acs.energyfuels.4c02933
Energy Fuels 2024, 38, 21456−21467

■ ASSOCIATED CONTENT

Supporting Information

The Supporting Information is available free of charge at https://pubs.acs.org/doi/10.1021/acs.energyfuels.4c02933.

Rietveld refined XRD results; cross-sectional FIB-SEM micrographs; EDS mapping; and fitted parameters of EIS spectra (PDF)

■ AUTHOR INFORMATION

Corresponding Authors

Sivaraj Pazhaniswamy − *Department of Materials, University of Oxford, OX1 3PH Oxford, U.K.; Bavarian Center for Battery Technology, Advanced Sustainable Polymers, Macromolecular Chemistry II, University of Bayreuth, Bayreuth 95440, Germany;* orcid.org/0000-0003-0241-4496; Email: sivarajmsc2@gmail.com, Sivaraj.Pazhaniswamy@materials.ox.ac.uk

Seema Agarwal − *Bavarian Center for Battery Technology, Advanced Sustainable Polymers, Macromolecular Chemistry II, University of Bayreuth, Bayreuth 95440, Germany;* orcid.org/0000-0002-3174-3152; Email: agarwal@uni-bayreuth.de

Authors

Gihoon Cha − *Fraunhofer Institute for Ceramic Technologies and Systems IKTS, 91301 Forchheim, Germany*

Sagar A. Joshi − *Bavarian Center for Battery Technology, Advanced Sustainable Polymers, Macromolecular Chemistry II, University of Bayreuth, Bayreuth 95440, Germany*

Abhilash Karuthedath Parameswaran − *Department of Physics and Electronics, Christ University, Bangalore 560029, India; Department of Inorganic Chemistry, University of Chemistry and Technology, 166 28 Prague 6, Czech Republic;* orcid.org/0000-0001-9469-3204

Rajan Jose − *Center for Advanced Intelligent Materials and Faculty of Industrial Sciences and Technology, Universiti Malaysia Pahang Al-Sultan Abdullah, 26300 Kuantan, Malaysia; Battery Research Center of Green Energy, Ming Chi University of Technology, 24301 New Taipei City, Taiwan;* orcid.org/0000-0003-4540-321X

Sabrina Pechmann − *Fraunhofer Institute for Ceramic Technologies and Systems IKTS, 91301 Forchheim, Germany*

Silke Christiansen − *Fraunhofer Institute for Ceramic Technologies and Systems IKTS, 91301 Forchheim, Germany*

Complete contact information is available at: https://pubs.acs.org/10.1021/acs.energyfuels.4c02933

Notes

The authors declare no competing financial interest.

■ ACKNOWLEDGMENTS

Author Sivaraj P thanks the Bavarian Centre for Battery Technology (BayBatt), University of Bayreuth, Bayreuth, Germany, for providing the necessary financial support through the Postdoctoral Research Fellowship to carry out the work. Dr. Abhilash K P thanks CHRIST University, Bangalore for providing the seed money to carry out the research.

■ REFERENCES

(1) Zhu, J.; Zhang, M.; Gai, Y.; Zeng, R.; Cai, Y.; Lu, D. Quickly form stable cathode/electrolyte interface of $LiNi_{0.5}Mn_{1.5}O_4$ (LNMO)/graphite high-voltage lithium ion cells by using tosylmethyl isocyanide (TosMIC) as electrolyte additive. *J. Power Sources* **2023**, *576*, 233227.

(2) Yang, Y.; Nie, Y.; Shen, Y.; Wei, J.; He, K.; Wen, Y.; Su, J. Alginate-Xylan Biopolymer as a multifunctional binder for 5 v High-Voltage LNMO electrodes. *ACS Appl. Mater. Interfaces* **2023**, *15* (21), 25909−25918.

(3) Guo, K.; Qi, S.; Wang, H.; Huang, J.; Wu, M.; Yang, Y.; Li, X.; Ren, Y.; Ma, J. High-Voltage electrolyte chemistry for lithium batteries. *Small Sci.* **2022**, *2* (5), 2100107.

(4) Huo, S.; Sheng, L.; Xue, W.; Wang, L.; Xu, H.; Zhang, H.; Su, B.; Lyu, M.; He, X. Challenges of stable ion pathways in Cathode electrode for All-Solid-State Lithium Batteries: A review. *Adv. Energy Mater.* **2023**, *13* (15), 2204343.

(5) Fu, T.; Lu, D.; Yao, Z.; Li, Y.; Luo, C.; Yang, T. C.; Liu, S.; Chen, Y.; Guo, Q.; Zheng, C.; Sun, W. Advances in modification methods and the future prospects of high-voltage spinel $LiNi_{0.5}Mn_{1.5}O_4$ - a review. *J. Mater. Chem. A* **2023**, *11* (26), 13889−13915.

(6) Konar, R.; Maiti, S.; Markovsky, B.; Sclar, H.; Aurbach, D. Exploring the capability of framework materials to improve Cathodes' performance for high-energy lithium-ion batteries. *Chem. Methods* **2024**, *4*, No. e202300039.

(7) Zhang, Y.; Wang, J.; Xue, Z. Electrode protection and electrolyte optimization via surface modification strategy for High-Performance Lithium batteries. *Adv. Funct. Mater.* **2024**, *34*, 2311925.

(8) Yang, J.; Liang, X.; Ryu, H.; Yoon, C. S.; Sun, Y. Ni-rich layered cathodes for lithium-ion batteries: From challenges to the future. *Energy Storage Mater.* **2023**, *63*, 102969.

(9) Hou, L.; Liu, Q.; Chen, X.; Yang, Q.; Mu, D.; Li, L.; Wu, F.; Chen, R. In-depth understanding of the deterioration mechanism and modification engineering of high energy density Ni-rich layered lithium transition-metal oxide cathode for lithium-ion batteries. *Chem. Eng. J.* **2023**, *465*, 142946.

(10) Sivaraj, P.; Abhilash, K. P.; Selvin, P. C. A critical review on electrochemical properties and significance of Orthosilicate-Based cathode materials for rechargeable Li/NA/MG batteries and hybrid supercapacitors. *ChemistrySelect* **2021**, *6* (43), 12036−12073.

(11) Pazhaniswamy, S.; Parameswaran, A. K.; Balakrishnan, N.; Goel, S.; Sofer, Z.; Yadav, S. K.; Panneerselvam, C. S. Prediction Clue on the fading capacity of Multi-Walled Carbon Nanotube-Decorated $Li_2(Fe_{1-X}Ti_X)SiO_4$/C High-Performance cathode materials. *Energy Fuels* **2021**, *35* (9), 8321−8333.

(12) Gao, Y.; Zhang, H.; Liu, X.-H.; Yang, Z.; He, X.; Li, L.; Qiao, Y.; Chou, S. Low-Cost Polyanion-Type sulfate cathode for Sodium-Ion battery. *Adv. Energy Mater.* **2021**, *11* (42), 2101751.

(13) Yang, Y.; Nie, Y.; Shen, Y.; Wei, J.; He, K.; Wen, Y.; Su, J. Alginate-Xylan Biopolymer as a multifunctional binder for 5 v High-Voltage LNMO electrodes. *ACS Appl. Mater. Interfaces* **2023**, *15* (21), 25909−25918.

(14) Zhao, H.; Lam, W. A.; Sheng, L.; Wang, L.; Bai, P.; Yang, Y.; Ren, D.; Xu, H.; He, X. Cobalt-Free Cathode Materials: Families and their Prospects. *Adv. Energy Mater.* **2022**, *12* (16), 2103894.

(15) Qureshi, Z. A.; Tariq, H. A.; Shakoor, R.; Kahraman, R.; AlQaradawi, S. Y. Impact of coatings on the electrochemical performance of LiNi0.5Mn1.5O4 cathode materials: A focused review. *Ceram. Int.* **2022**, *48* (6), 7374−7392.

(16) Guo, J.; Sun, X.; Xu, J.; Bian, Y.; Wang, Y.; Jin, P.; Wang, L.; Liang, G. Flavone as a novel multifunctional electrolyte additive to improve the cycle performance of high-voltage $LiNi_{0.5}Mn_{1.5}O_4$ batteries. *Appl. Surf. Sci.* **2023**, *616*, 156534.

(17) Lee, D.; Cui, Z.; Goodenough, J. B.; Manthiram, A. Interphase stabilization of $LiNi_{0.5}Mn_{1.5}O_4$ Cathode for 5 V-Class All-Solid-State batteries. *Small* **2024**, *20* (2), 2306053.

(18) Huang, W.; Yan, L.; Zhang, L.; Zhang, X.; Wu, Z.; Zhu, C.; Fang, Z.; Yang, K. Bifunctional urea surface-modified high voltage $LiNi_{0.5}Mn_{1.5}O_4$ cathode for enhanced electrochemical performance. *Electrochim. Acta* **2023**, *458*, 142525.

(19) Liu, J.; Yuan, M.; Li, Z.; Wang, L.; Yan, J.; Peng, J.; Ou, S.; Xu, J. Enhancing structure and cycling stability of single crystal $LiNi_{0.5}Mn_{1.5}O_4$ cathode via multifunctional MXene surface modification. *J. Energy Storage* **2024**, *76*, 109785.
(20) Zhu, Z.; Xu, S.; Wang, Z.; Yan, X.; Xu, G.; Huang, Y.; Wu, Y.; Zhang, Y.; Li, J. Avoiding electrochemical indentations: a CNT-cocooned $LiCoO_2$ electrode with ultra-stable high-voltage cycling. *Energy Environ. Sci.* **2024**, *17* (16), 6102−6112.
(21) Xiong, X.; Sun, R.; Yan, W.; Qiao, Q.; Zhu, Y.; Liu, L.; Fu, L.; Yu, N.; Wu, Y.; Wang, B. A lithiophilic AlN-modified copper layer for high-performance lithium metal anodes. *J. Mater. Chem. A* **2022**, *10* (26), 13814−13820.
(22) Heng, Y. L.; Gu, Z. Y.; Guo, J. Z.; Yang, X. T.; Zhao, X. X.; Wu, X. L. Research progress on the surface/interface modification of high-voltage lithium oxide cathode materials. *Energy Mater.* **2022**, *2* (3), 200017.
(23) Li, L.; Duan, H.; Li, J.; Zhang, L.; Deng, Y.; Chen, G. Toward high performance all-solid-state lithium batteries with high-voltage cathode materials: design strategies for solid electrolytes, cathode interfaces, and composite electrodes. *Adv. Energy Mater.* **2021**, *11* (28), 2003154.
(24) Pazhaniswamy, S.; Joshi, S. A.; Hou, H.; Parameswaran, A. K.; Agarwal, S. Hybrid polymer electrolyte encased cathode particles Interface-Based Core−Shell structure for High-Performance room Temperature All-Solid-State batteries. *Adv. Energy Mater.* **2023**, *13*, 2202981.
(25) Shu, Y.; Xie, Y.; Yan, W.; Meng, S.; Sun, D.; Jin, Y.; He, K. Synergistic effect of surface plane and particle sizes on the electrochemical performance of $LiNi_{0.5}Mn_{1.5}O_4$ cathode material via a facile calcination process. *J. Power Sources* **2019**, *433*, 226708.
(26) Wang, J.; Nie, P.; Xu, G.; Jiang, J.; Wu, Y.; Fu, R.; Dou, H.; Zhang, X. High-Voltage $LiNi_{0.45}Cr_{0.1}Mn_{1.45}O_4$ Cathode with Super-long Cycle Performance for Wide Temperature Lithium-Ion Batteries. *Adv. Funct. Mater.* **2018**, *28* (4), 1704808.
(27) Gao, C.; Liu, H.; Zhang, J.; Guo, Z.; Huang, H. Simplified crystal grain boundary engineering of solid electrolyte-infused $LiNi_{0.5}Mn_{1.5}O_4$ cathodes for high cycling stability lithium-ion batteries. *J. Power Sources* **2023**, *582*, 233434.
(28) Ghosh, S.; Mahapatra, M.; Bhowmik, S.; Garlapati, K. K.; Martha, S. K. Soft carbon integration for prolonging the cycle life of $LiNi_{0.5}Mn_{1.5}O_4$ Cathode. *ACS Appl. Energy Mater.* **2023**, *6* (18), 9390−9399.
(29) Reddy, M. V.; Cheng, H. Y.; Tham, J. H.; Yuan, C. Y.; Goh, H. L.; Chowdari, B. V. R. Preparation of $Li(Ni_{0.5}Mn_{1.5})O_4$ by polymer precursor method and its electrochemical properties. *Electrochim. Acta* **2012**, *62*, 269−275.
(30) Karunawan, J.; Suryadi, P. N.; Mahfudh, L.; Santosa, S. P.; Sumboja, A.; Iskandar, F. Truncated octahedral shape of spinel $LiNi_{0.5}Mn_{1.5}O_4$ via a Solid-State method for Li-Ion batteries. *Energy Fuels* **2023**, *37* (1), 754−762.
(31) Li, T.; Chen, Z.; Bai, F.; Li, C.; Li, Y. Diluted low concentration electrolyte for interphase stabilization of high-voltage $LiNi_{0.5}Mn_{1.5}O_4$ cathode. *J. Energy Chem.* **2023**, *81*, 404−409.
(32) Huang, W.; Yan, L.; Zhang, L.; Zhang, X.; Wu, Z.; Zhu, C.; Fang, Z.; Yang, K. Bifunctional urea surface-modified high voltage $LiNi_{0.5}Mn_{1.5}O_4$ cathode for enhanced electrochemical performance. *Electrochim. Acta* **2023**, *458*, 142525.
(33) Huang, J.; Cheng, C.-Y.; Lai, Y.; Iputera, K.; Chung, R.-J.; Liu, R. Engineering Cathode−Electrolyte interface of High-Voltage spinel $LiNi_{0.5}Mn_{1.5}O_4$ via Halide Solid-State Electrolyte Coating. *ACS Appl. Mater. Interfaces* **2023**, *15* (34), 40648−40655.
(34) Parameswaran, A. K.; Azadmanjiri, J.; Palaniyandy, N.; Pal, B.; Palaniswami, S.; Dekanovsky, L.; Wu, B.; Sofer, Z. Recent progress of nanotechnology in the research framework of all-solid-state batteries. *Nano Energy* **2023**, *105*, 107994.
(35) Jiao, X.; Rao, L.; Yap, J.; Yu, C.-Y.; Kim, J. H. Stabilizing cathode-electrolyte interphase of $LiNi_{0.5}Mn_{1.5}O_4$ high-voltage spinel by blending garnet solid electrolyte in lithium-ion batteries. *J. Power Sources* **2023**, *561*, 232748.
(36) Park, N. R.; Li, Y.; Yao, W.; Zhang, M.; Han, B.; Mejia, C.; Sayahpour, B.; Shimizu, R.; Bhamwala, B.; Dang, B.; Kumakura, S.; Li, W.; Meng, Y. S. Understanding the role of lithium borate as the surface coating on high voltage single crystal $LiNi_{0.5}Mn_{1.5}O_4$. *Adv. Funct. Mater.* **2024**, *34* (13), 2312091.
(37) Zhang, J.; Cao, L.; Li, J.; Yang, M.; Yu, J.; Cheng, Y.; Huang, Y.; Xia, Y. One thousandth of quaternity slurry additive enables one thousand cycle of 5V LNMO cathode. *Energy Storage Mater.* **2024**, *64*, 103060.
(38) Liu, S.; Liu, X.; Ren, D.; Li, T.; Yi, L.; Liu, W.; Xu, J.; Tan, T.; Zhang, J.; Hou, Y.; Guo, Y.; Zhu, G.; Yin, S.; Yuan, G.; Weng, Y.; Ma, G.; Peng, Z.; Zheng, X.; Yin, W.; Lu, L.; Ouyang, M. Inhibit the strain accumulation for 5 V spinel cathode by mitigating the phase separation during high voltage stage. *Nano Energy* **2024**, *121*, 109215.
(39) Li, Y.; Li, X.; Liu, L.; Li, C.; Xing, L.; He, J.; Li, W. Multifunctional Silane Additive Enhances Inorganic−Organic Compatibility with F-rich Nature of Interphase to Support High-Voltage $LiNi_{0.5}Mn_{1.5}O_4$/graphite Pouch Cells. *Adv. Funct. Mater.* **2024**, *34* (19), 2312921.
(40) Zhang, Y.; Liu, F.; Song, T.; Pei, Y.; Wang, X.; Wu, X.; Xiao, M.; Deng, Q.; Long, B. Converting commercial MnO2 into Co-doped $LiNi_{0.5}Mn_{1.5}O_4$ with adjustable disordered/ordered phase ratio by a quaternary molten salt. *Chem. Eng. J.* **2024**, *480*, 148369.
(41) Liu, J.; Yuan, M.; Liu, H.; Li, Z.; Wang, L.; Yan, J.; Peng, J.; Ou, S.; Xu, J. Improving the safety performance of $LiNi_{0.5}Mn_{1.5}O_4$ through strategies of doping, coating and oxygen self-absorption additive. *J. Power Sources* **2024**, *591*, 233840.
(42) Sun, H.; Hu, A.; Spence, S.; Kuai, C.; Hou, D.; Mu, L.; Liu, J.; Li, L.; Sun, C.; Sainio, S.; Nordlund, D.; Luo, W.; Huang, Y.; Lin, F. Tailoring Disordered/Ordered phases to revisit the degradation mechanism of High-Voltage $LiNi_{0.5}Mn_{1.5}O_4$ spinel cathode materials. *Adv. Funct. Mater.* **2022**, *32* (21), 2112279.
(43) Liang, G.; Peterson, V. K.; See, K. W.; Guo, Z.; Pang, W. K. Developing high-voltage spinel $LiNi_{0.5}Mn_{1.5}O_4$ cathodes for high-energy-density lithium-ion batteries: current achievements and future prospects. *J. Mater. Chem. A* **2020**, *8* (31), 15373−15398.
(44) Yu, X.; Yu, W. A.; Manthiram, A. Advances and prospects of high-voltage spinel cathodes for lithium-based batteries. *Small Methods* **2021**, *5* (5), 2001196.

https://doi.org/10.1021/acs.energyfuels.4c02933
Energy Fuels 2024, 38, 21456−21467